ELSEVIER

Journal of Computational and Applied Mathematics 149 (2002) 439–456

JOURNAL OF COMPUTATIONAL AND APPLIED MATHEMATICS

www.elsevier.com/locate/cam

Conjugate filter approach for solving Burgers' equation ☆

G.W. Wei[a,b,*], Yun Gu[b]

[a] *Department of Mathematics, Michigan State University, East Lansing, MI 48824, USA*
[b] *Department of Computational Science, National University of Singapore, Singapore 117543, Singapore*

Received 20 August 2001; received in revised form 11 December 2001

Abstract

We propose a novel scheme for solving Burgers' equation with all possible values of Reynolds numbers. A low-pass filter is introduced to intelligently eliminate the high frequency errors produced by its conjugate high-pass filters. All conjugate filters are derived from one generating function and have essentially the same degree of regularity, smoothness, time-frequency localization, effective support and bandwidth. Computational accuracy is tested by using both a linear hyperbolic equation and Burgers' equation at a moderately high Reynolds number for which analytical solution is available. The ability of shock-capturing is validated by using discontinuous initial values. Excellent numerical results indicate that the proposed scheme is efficient, robust and reliable for solving Burgers' equation and for shock capturing.

1. Introduction

The fundamental equation for the description of complex fluid flow is the Navier–Stokes equation, for which the full solution is still extremely difficult in the full domain of physical interest. Burgers' equation [4] is an important simple model for the understanding of physical flows. Simulation of Burgers' equation is a natural first step towards developing methods for the computation of complex flows. In the past a few decades, it appears customary to test new approaches in computational fluid dynamics by applying them to Burgers' equation with a variety of initial values. Jamet and Bonnerot solved Burgers' equation by using an isoparametric rectangular space–time finite element [14]. Jain and Holla [13] developed a cubic spline approach for coupled Burgers' equations. Varoglu and Finn [18] proposed an isoparametric space–time finite element method for solving Burgers' equation, utilizing the hyperbolic differential equation associated with Burgers' equation. They obtained very

☆ This paper is dedicated to Robert F. Snider on the occasion of his 70th birthday.

* Corresponding author. Tel.: +874-6589; fax: +774-6756.
E-mail address: cscweigw@nus.edu.sg (G.W. Wei).

0377-0427/02/$ - see front matter
PII: S0377-0427(02)00488-0

high accuracy and numerical stability with a reasonable number of elements and time steps. Their method was compared with a least square weak formulation of the finite element method by Nguyen and Reynen [17]. Caldwell et al. [5] further developed the finite element method to allow a different size of elements at each stage based on the feed back from the previous step. A generalized boundary element approach was proposed by Kakuda and Tosaka [16]. These authors tabulated their accurate results for moderate Reynolds numbers and compared their results with those of Varoglu and Finn [18] and of Nguyen and Reynen [17]. A bidimensional Tau-element method was developed by Ortiz and Pun for solving Burgers' equation with accurate results. Bar-Yoseph et al. discussed a number of space–time spectral element methods for solving Burgers' equation [2]. Arina and Canuto [1] treated Burgers' equation by a self-adaptive, domain decomposition method called the χ-formulation. Various finite difference schemes for Burgers' equation were compared by Biringen and Saati [3]. Recently, Wei et al. [25] have developed an accurate solver for Burgers' equation in one and two space dimensions. Most recently, Hon and Mao [12] have compared performance of their adaptive multiquadric scheme with many other computational methods. It is not our purpose to exhaust the literature. Despite of much effort, numerical solution of Burgers' equation is still a nontrivial task especially at very high Reynolds numbers where the nonlinear advection leads to shock waves. In fact, Burgers' inviscid shocks plague many standard computational algorithms. Obviously, to solve Burgers' equation at a high Reynolds number or with discontinuous initial values, a scheme which is capable of shock-capturing is indispensable.

The purpose of this paper is to report a novel scheme for solving Burgers' equation for all possible values of Reynolds numbers and for shock capturing. We propose a conjugate filter oscillation reduction (CFOR) scheme to solve Burgers' equation. As the first and second derivatives are approximated by using two high-pass filters, the numerical errors of the high-pass filters at the high frequency region lead to oscillations near Burgers' shock wave front. The proposed idea is to effectively eliminate such oscillations by using a conjugate low-pass filter. This set of high-pass and low-pass filters are conjugated in the sense that they are derived from one generating function and consequently have essentially the same degree of regularity, smoothness, time-frequency localization, effective support and bandwidth. In the present work, all conjugated filters are constructed by using a discrete singular convolution (DSC) algorithm [20–22], which was proposed as a potential approach for the computer realization of singular integrations. The theory of distributions and theory of wavelet analyses form the mathematical foundation for the DSC. Sequences of approximations to the singular kernels of Hilbert type, Abel type and delta type were constructed. Applications are discussed to analytical signal processing, Radon transform and surface interpolation. Numerical solutions to differential equations are formulated via singular kernels of the delta type. By appropriately choosing DSC kernels, the DSC approach exhibits global methods' accuracy for integration and local methods' flexibility in handling complex geometries and boundary conditions. The DSC algorithm was very successful in solving the Navier–Stokes equation [23,19] and in vibration analysis [24]. In particular, the analysis of plates vibrating at extremely high frequency and with densely distributed internal supports is a very challenging task, for which conventional methods have encountered a great deal of numerical instability. The DSC algorithm is the only available method for resolving these problems [26].

This paper is organized as follows. Section 2 is devoted to computational methodology. Conjugate filters are constructed via the DSC algorithm. A scheme for oscillation reduction is proposed. Numerical applications are presented in Section 3. A few benchmark examples are employed to test

the proposed approach. Results are compared with those in the literature. This paper ends with a conclusion.

2. Methodology

In this section, conjugated filters are constructed by using the discrete singular convolution (DSC) algorithm. A new oscillation reduction scheme is introduced after describing the DSC formalism.

2.1. Conjugated filters

As a special class of mathematical transformations, singular convolutions appear in many science and engineering problems. It is most convenient to discuss singular convolutions in the context of the theory of distributions. The latter has a significant impact in mathematical analysis. It provides a rigorous justification for a number of informal manipulations in engineering and physics, and has significant influence many mathematical disciplines, such as operator calculus, differential equations, functional analysis, harmonic analysis and transformation theory. Let T be distribution and $\eta(t)$ be an element of the space of test functions. A singular convolution is defined as

$$F(t) = (T * \eta)(t) = \int_{-\infty}^{\infty} T(t-x)\eta(x)\,\mathrm{d}x. \tag{1}$$

Here $T(t-x)$ is a singular kernel. Depending on the form of the kernel T, the singular convolution is the central issue for a wide range of science and engineering problems, such as Hilbert transform, Abel transform and Radon transform. In the present study, only singular kernels of the delta type are required

$$T(x) = \delta^{(n)}(x) \quad (n = 0, 1, 2, \ldots). \tag{2}$$

Here, kernel $T(x) = \delta(x)$ is of particular importance for interpolation of surfaces and curves. Higher-order kernels, $T(x) = \delta^{(n)}$, $(n = 1, 2, \ldots)$ are essential for numerically solving partial differential equations and for image processing, noise estimation, etc. However, since these kernels are singular, they cannot be directly digitized in computers. Hence, the singular convolution (1), is of little numerical merit as it is. To avoid the difficulty of using singular expressions directly in computer, we construct sequences of approximations $\{T_\alpha\}$ to the distribution T

$$\lim_{\alpha \to \alpha_0} T_\alpha(x) \to T(x), \tag{3}$$

where α_0 is a generalized limit. Obviously, in the case of $T(x) = \delta(x)$, each element in the sequence, $T_\alpha(x)$, is a delta sequence kernel. With a sufficiently smooth approximation, it is useful to consider a discrete singular convolution of the form

$$F_\alpha(t) = \sum_k T_\alpha(t - x_k) f(x_k), \tag{4}$$

where $F_\alpha(t)$ is an approximation to $F(t)$ and $\{x_k\}$ is an appropriate set of discrete points on which the DSC (4) is well defined. Note that, the original test function $\eta(x)$ has been replaced by an ordinary function $f(x)$ because kernels T_α are restricted to a set of well-behaved ones.

A typical example is Shannon's delta kernel, which is given by the following (inverse) Fourier transform of the characteristic function, $\chi[-\alpha,\alpha]$,

$$\delta_\alpha(x)=\frac{1}{2\pi}\int_{-\infty}^{\infty}\chi_{[-\alpha,\alpha]}e^{i\xi x}\,d\xi=\frac{\sin(\alpha x)}{\pi x}. \tag{5}$$

For the purpose of digital computations, it is necessary to discretize delta kernels. To this end, we examine a sampling basis given by Shannon's delta kernel

$$S_k(x)=\frac{\sin\pi(x-x_k)}{\pi(x-x_k)}. \tag{6}$$

Such a sampling basis is obviously interpolative

$$S_k(x_l)=\delta_{k,l}, \tag{7}$$

where $\delta_{k,l}$ is the Kronecker delta function. Computationally, being interpolative is desirable for numerical accuracy and simplicity. In fact, this sampling basis is also an element of the Paley–Wiener reproducing kernel Hilbert space. It provides a discrete representation of every (continuous) function in B_π^2, that is

$$f(x)=\sum_{k\in Z}f(x_k)S_k(x),\quad \forall k\in B_\pi^2. \tag{8}$$

This is Shannon's sampling theorem and it means that one can recover a continuous bandlimited L^2 function from a set of discrete values. Shannon's sampling theorem had a great impact on information theory, signal and image processing because the Fourier transform of Shannon's delta kernel is an ideal low-pass filter, see Fig. 1. It is, in fact, an infinite impulse response (IIR) low-pass filter. For numerical computations, Eq. (8) can never be realized because it requires infinitely many sampling points. A truncation is required in practical computations. Unfortunately, Shannon's delta kernel decays slowly and leads to substantial truncation errors. According to the theory of distributions, the smoothness, regularity and localization of a tempered distribution can be improved by regularization with a function of the Schwartz class. We apply this principle to regularize approximate convolution kernels

$$\delta_{\sigma,\alpha}(x)=R_\sigma(x)\delta_\alpha(x)\quad(\sigma>0), \tag{9}$$

where R_σ is a Gaussian regularizer $R_\sigma(x)=\exp[-x^2/2\sigma^2]$. The Gaussian regularizer is a Schwartz class function and thus, the expression in Eq. (9) can be applied to tempered distributions. Numerically, the truncation error is dramatically reduced by the use of the delta regularizer. The regularized Shannon's delta kernel (RSK) on an arbitrary grid is given by

$$\delta_{\sigma,\Delta}(x-x_k)=\frac{\sin\pi/\Delta(x-x_k)}{\pi/\Delta(x-x_k)}\,e^{-(x-x_k)^2/2\sigma^2}, \tag{10}$$

where Δ is the grid spacing. Since the truncation error can be dramatically reduced by the Gaussian regularizer, the expression given by Eq. (10) is practically a finite impulse response (FIR) low-pass filter and has a compact support for numerical interpolation.

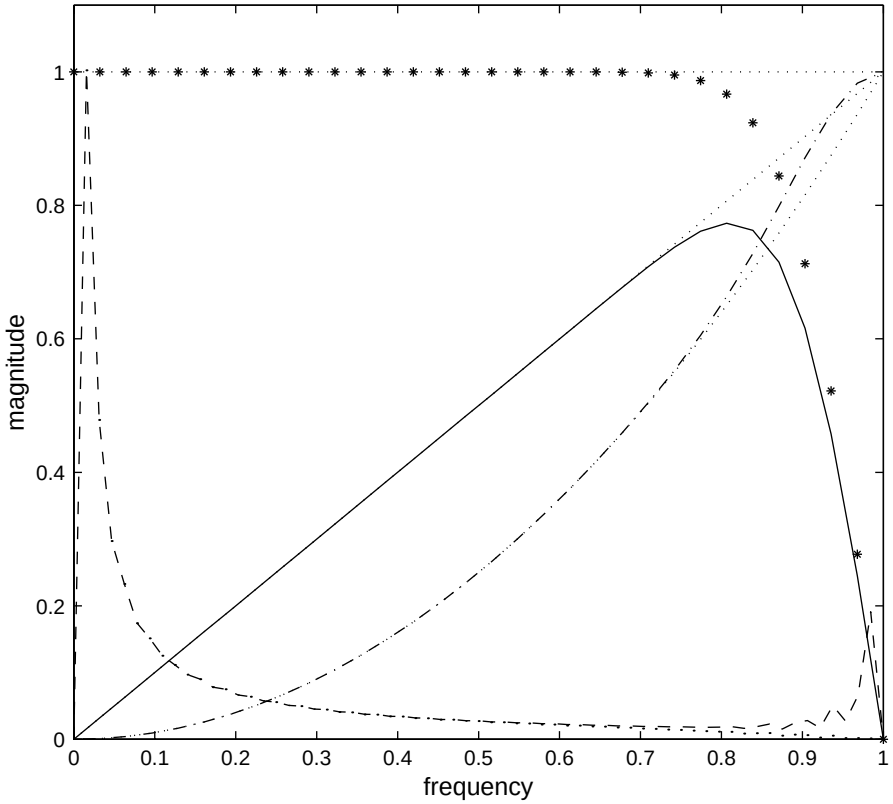

Fig. 1. Graph of the frequency responses of the conjugated DSC filters (in the unit of π/Δ). The maximum amplitude is normalized to the unit. Stars: conjugate low-pass filter; solid line: first-order high-pass filter; Dash-dots: second-order high-pass filter; Small dots: ideal filters; Dashed line: Fourier image of the numerical solution of Burgers' equation ($t = 0.5$, $\mathrm{Re} = 10^5$) with oscillations; Big dots: Fourier image of the numerical solution obtained by using the CFOR scheme.

As such, a function and its nth order derivative are approximated in the DSC algorithm as

$$f^{(n)}(x) \approx \sum_{k=-M}^{M} \delta^{(n)}_{\sigma,\Delta}(x - x_k) f(x_k) \quad (n = 0, 1, 2, \ldots), \tag{11}$$

where $\delta_{\sigma,\Delta}(x - x_k)$ is a collective symbol for any (regularized) delta kernel, and $2M + 1$ is the computational bandwidth. The higher-order derivative terms $\delta^{(n)}_{\sigma,\Delta}(x - x_k)$ are given by

$$\delta^{(n)}_{\sigma,\Delta}(x - x_k) = \left(\frac{d}{\mathrm{d}x}\right)^n \delta_{\sigma,\Delta}(x - x_k). \tag{12}$$

Here, the differentiation can be carried out analytically. Numerical solution of differential equations can be easily implemented in a collocation scheme by using Eq. (11). Expressions in Eq. (12) are high-pass filters as their filter responses vanish at zero frequency. Obviously, both the low-pass filter and high-pass filters are constructed by using the DSC delta kernel and thus, have essentially the same degree of regularity, smoothness, time-frequency localization, effective support and bandwidth. Therefore, we refer this set of filters as conjugated filters.

2.2. Oscillation reduction scheme

Fig. 1 shows the frequency responses of the conjugate DSC low-pass filter, the first- and second-order high-pass filters at $\sigma = 3.2\Delta$. Indeed, all conjugated filters have essentially the same effective bandwidth, which is about $0.7\pi/\Delta$. Below $0.7\pi/\Delta$, frequency responses of all the conjugated filters are essentially exact. However, in the very high frequency region, frequency response of both the low-pass filter and the first-order high-pass filter is underestimated, whereas that of the second-order high-pass filter is overestimated. The proposed idea is to use the conjugate low-pass filter to intelligently eliminate the high frequency errors produced by the conjugate high-pass filters during a numerical computation. As a consequence, the resulting numerical calculations are correct and reliable for frequency below the effective bandwidth of conjugated filters. Coordinate space implementation and numerical demonstration of this idea are presented in the rest of this paper.

To solve Burgers' equation at very high Reynolds numbers, let us consider a system of essentially hyperbolic type in one dimension (1D)

$$\begin{aligned} &u_t + f(u)_x = \varepsilon u_{xx}, \\ &u(x,0) = u_0(x), \end{aligned} \tag{13}$$

where u is a scalar field, f is a hyperbolic mapping, and ε is a small parameter. At the limit of $\varepsilon \to 0$, the system reduces to standard hyperbolic conservation laws and can induce severe spurious oscillations in a normal solution procedure.

The control of oscillations can be accomplished in a number of ways. For example, Godunov algorithms [9], up-wind schemes, essentially nonoscillatory (ENO) schemes [11], weighted ENO schemes [15] and filter schemes [8] are standard methods for handling oscillations. In the present work, we propose an alternative approach which makes use of the conjugate low-pass filter, Eq. (10). Since the peak of undesired oscillations resides outside the effective bandwidth of the conjugate low-pass filter as shown in Fig. 1, it can be removed by the filtering via the conjugate low-pass filter. To eliminate oscillations and preserve the true solution effectively, we design the following conjugate filter oscillation reduction (CFOR) scheme

$$v^{n+1} = H(u^n), \tag{14}$$

$$u^{n+1} = \begin{cases} v^{n+1} & \delta\mathscr{W}^{n+1} < \eta, \\ G(v^{n+1}) & \delta\mathscr{W}^{n+1} \geqslant \eta, \end{cases} \tag{15}$$

where H refers to the treatment by DSC high-pass filters, $\delta^{(q)}_{\sigma,\pi/\Delta}$ $(q = 1, 2)$, and G represents the convolution with the DSC low-pass filter $\delta_{\sigma,\pi/\Delta}$. Here η is a threshold value, and $\mathscr{W}$ is a high-pass measure, which is defined via a multiscale wavelet transform of a set of discrete function values $\{v(x_k, t_n)\}_{k=1}^N$ at time t_n as

$$\|\mathscr{W}^n\| = \sum_m \|\mathscr{W}^n_m\|, \tag{16}$$

where $\|\mathscr{W}^n_m\|$ is given by a convolution with a wavelet ψ_{mj} of scale m

$$\|\mathscr{W}^n_m\| = \sum_k |\sum_j \psi_{mj}(x_k) u^n(x_j)|. \tag{17}$$

Conjugate low-pass filters are adaptively implemented whenever the difference of high pass measure accesses a positive alarm threshold η

$$\delta \mathscr{W}^{n+1} = \|\mathscr{W}^{n+1}\| - \|\mathscr{W}^{n}\| \geqslant \eta. \tag{18}$$

In the present tests, we use the Haar wavelet of one scale. The choice of η depends on the time increment Δt and the grid size Δx.

Note that DSC low-pass filters are interpolative. Therefore, it is necessary to implement them through prediction $[u(x_k) \to u(x_{k+1/2})]$ and restoration $[u(x_{k+1/2}) \to u(x_k)]$. The use of such adaptive filters is computationally efficient because it does not need to judge local flow directions as a Riemann solver does. The implementation of DSC filters is very simple as explicitly shown in Eq. (11). We use the standard fourth-order Runge–Kutta scheme for time advancement in the present work, although an implicit scheme may also be easily implemented. It is straightforward to extend the conjugated filters to higher spatial dimensions by tensorial products.

3. Applications

In this section, we validate the proposed scheme for linear equation of the hyperbolic type before the scheme is applied to Burgers' equation. We hope that experience learned from solving a linear equation is valuable for tackling a nonlinear one. In all the present calculations, we choose $M = 32$ and $\sigma/\Delta = 3.5$ for normal computations (including predictions). Parameter $\eta = 0.001$ is selected to control the possible use of low-pass filtering, in which, restoration is done with DSC parameters $M = 31$ and $\sigma/\Delta = 0.75$.

3.1. A linear equation

The difficulty of solving Burgers' equation at arbitrary high Reynolds numbers lies in the possible spurious oscillations. The capability of shock-capturing is the key for any potential scheme. To validate a scheme for shock-capturing, it is standard to consider a linear equation of hyperbolic type [15]

$$\begin{aligned} &u_t + u_x = 0, \quad -1 < x < 1, \\ &u(x,0) = u_0(x), \quad \text{periodic}. \end{aligned} \tag{19}$$

The exact solution is a family of traveling waves given by $u(x,t) = u_0(x-t)$ for $t \geqslant 0$. The solution $u(x,t)$ is constant along the characteristics given by a ray $x - t = x_0$. We investigate the performance of the proposed scheme by using three sets of initial data $u_0(x)$. The first two examples are designed to test the computational accuracy and to compare with standard methods in the literature. The third example is discontinuous and is used to examine the shock-capturing ability of the proposed scheme.

Example 1. The first initial value is given by

$$u_0(x) = \sin^4(\pi x). \tag{20}$$

Table 1
Comparison of errors and numerical orders of four numerical schemes

Method	N	L_∞ errors	L_∞ order	L_1 errors	L_1 order
	20	7.31(− 02)	—	3.29(− 02)	—
WENO-RF-4	40	2.48(− 02)	1.56	9.99(− 03)	1.72
	80	4.60(− 03)	2.43	1.44(− 03)	2.79
	20	1.08(− 01)	—	4.91(− 02)	—
WENO-RF-5	40	8.90(− 03)	3.60	3.64(− 03)	3.75
	80	1.80(− 03)	2.31	5.00(− 04)	2.86
	20	5.23(− 02)	—	3.53(− 02)	—
Central-5	40	2.47(− 03)	4.40	1.52(− 03)	4.46
	80	8.23(− 05)	4.89	5.09(− 05)	4.90
	20	1.00(− 09)	—	4.12(− 10)	—
CFOR	40	2.07(− 15)	18.88	1.11(− 16)	21.82
	80	8.23(− 16)	1.33	3.44(− 17)	1.69

This problem is valuable since it is analytically solvable and has been considered by previous authors to test their shock-capturing schemes [15]. The errors and numerical orders of the proposed scheme at time $t=1$ are listed in Table 1, and compared with those of three other standard methods [15]. Here N is the total number of cells, and $\Delta t/\Delta x$ is optimized. The fourth-order weighted essentially nonoscillatory scheme with Roe's flux splitting and entropy fix (WENO-RF-4) is a quite sophisticated shock-capturing scheme and is popularly used in the field of hyperbolic conservation laws. The WENO-RF-5, an accuracy-enhanced version of WENO-RF-4, is often regarded as the state of art scheme for shock-capturing. The performance of both schemes, as well as that of the fifth-order central difference scheme, was reported in the literature [15] for Eq. (20). It is seen that the DSC-based CFOR scheme yields a very high accuracy even for a coarse grid ($N=20$). It reaches the machine precision with a total of 40 grid points. The largest L_1 order of CFOR scheme is about 22, in comparing to about 4 for the WENO-RF-5 scheme. The accuracy of CFOR at 80 grid points is obviously limited by the double precision algorithm used in the computation.

Example 2. We next consider a Gaussian wave packet given by

$$u_0(x) = \cos[k\pi(x - x_0)]\mathrm{e}^{-(x-x_0)^2/2\sigma_0^2}, \tag{21}$$

where parameter k can be adjusted to give a more oscillatory wave, $\sigma_0=0.1$ is a constant controlling the width of the wave packet and $x_0 = 0$ is the initial center of the wave packet. This problem is interesting because real-world waves are both bandlimited and time-limited. Exact solution of the problem is the same wave packet moving to the right with velocity 1. We solve the problem by using three sets of grid points ($N=50, 100$ and 200) and three different k values ($k=5, 10$ and 15). The time increment is fixed as small as $\Delta t = 10^{-5}$ so that most errors are due to the DSC spatial discretization. Errors and numerical orders of the CFOR scheme for propagating the wave packets

are listed in Table 2 for $t = 2, 4$ and 6, which correspond to period 1, 2 and 3, respectively. When $k = 5$, some numerical orders with respect to mesh refinements are as high as 30. Obviously, the reported accuracy is limited by the double precision algorithm when the grid is refined to $N = 200$. Even for $k = 15$, the computed numerical orders are still very high in both the first and second mesh refinements. This indicates that the CFOR scheme is extremely accurate in solving the wave packet problem. For a comparison, both exact wave packets and numerical solutions obtained with $N = 100$, $t = 6$ are depicted in Fig. 2 for $k = 5, 10$ and 15. Obviously, there is no visual difference between the exact solutions and the CFOR results.

Example 3. Finally, we test the proposed scheme by using the following piecewise continuous initial value

$$u(x,0) = \begin{cases} 1, & 0 \leqslant x \leqslant 0.2, \\ 4x - \frac{6}{10}, & 0.2 < x \leqslant 0.4, \\ -4x + \frac{52}{20}, & 0.4 \leqslant x < 0.6, \\ 1, & 0.6 \leqslant x \leqslant 0.8, \\ 0, & \text{otherwise.} \end{cases} \tag{22}$$

This is a case with the so-called contact discontinuities and is quite difficult to solve in hyperbolic conservation laws. The discontinuity in the initial value may lead to severe spurious oscillations and shock-capturing ability is crucial for solving this problem. In particular, the intersections of two lines at $x = 0.2$ and 0.6 are difficult to resolve. Exact solution is given by the initial value moved with velocity 1 to the right. In Fig. 3, numerical solutions are given at $t = 8$. Obviously, the CFOR scheme performs extremely well for this case.

3.2. Burgers' equation

Having established our confidence for using the proposed scheme for treating the linear equation with various initial values, we pursue with the solution of Burgers' equation [4]

$$\frac{\partial u}{\partial t} + u\frac{\partial u}{\partial x} = \frac{1}{\mathrm{Re}}\frac{\partial^2 u}{\partial x^2}, \tag{23}$$

where $u(x,t)$ is the dependent variable resembling the flow velocity and Re is the Reynolds number characterizing the size of viscosity. The competition between the nonlinear advection and the viscous diffusion is controlled by the value of Re in Burgers' equation, and thus determines the behavior of the solution.

To test the proposed scheme for solving Burgers' equation, three standard benchmark problems are employed in this subsection. These problems are designed to explore the computational accuracy, stability, and shock-resolving capability of the CFOR scheme.

Example 1. We first consider Eq. (23) with the following initial-boundary conditions

$$u(x,0) = \sin(\pi x),$$
$$u(0,t) = u(1,t) = 0. \tag{24}$$

Table 2
Errors for solving the linear equation with Gaussian wave packets

k	N	$t=2$				$t=4$				$t=6$			
		L_1 error	L_1 order	L_∞ error	L_∞ order	L_1 error	L_1 order	L_∞ error	L_∞ order	L_1 error	L_1 order	L_∞ error	L_∞ order
	50	1.12e-05	—	2.19e-05	—	2.11e-05	—	3.83e-05	—	2.83e-05	—	5.04e-05	—
5	100	1.41e-14	29.57	5.80e-14	28.49	2.15e-14	29.87	9.09e-14	28.65	2.72e-14	29.95	1.66e-13	28.18
	200	8.34e-15	0.75	5.01e-14	0.21	1.34e-14	0.68	1.19e-13	-0.39	1.68e-14	0.70	1.47e-13	0.18
	50	3.22e-03	—	5.71e-03	—	5.24e-03	—	8.12e-03	—	6.45e-03	—	1.03e-02	—
10	100	8.21e-12	28.55	4.34e-11	26.97	1.64e-11	28.25	8.69e-11	26.48	2.46e-11	27.97	1.30e-10	26.34
	200	1.37e-14	9.23	1.04e-13	8.71	2.29e-14	9.48	1.92e-13	8.82	2.50e-14	9.94	1.63e-13	9.64
	50	1.07e-01	—	1.64e-01	—	1.29e-01	—	2.15e-01	—	1.52e-01	—	2.25e-01	—
15	100	5.96e-09	24.10	2.98e-08	22.39	1.19e-08	23.37	5.95e-08	21.78	1.79e-08	23.02	8.93e-08	21.26
	200	1.54e-14	18.56	8.00e-14	18.51	2.36e-14	18.94	1.57e-13	18.53	3.34e-14	19.03	1.54e-13	19.15

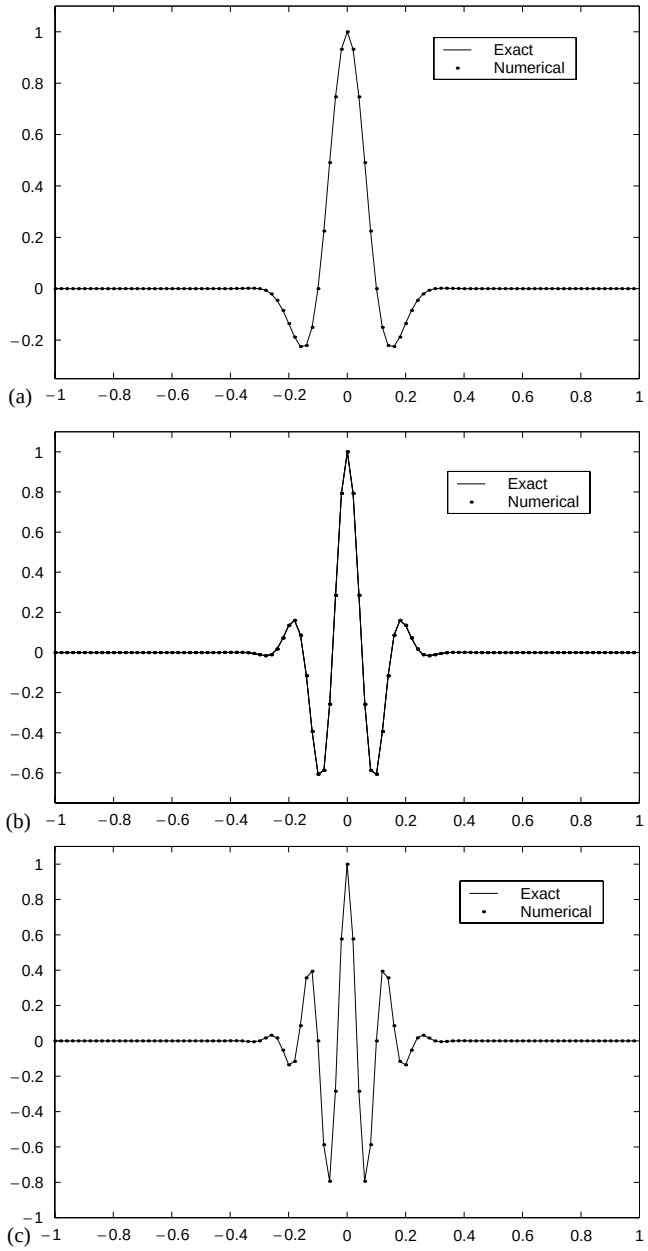

Fig. 2. Time evolution of Gaussian wave packets ($t = 6$, $\Delta x = 0.02$ and $\Delta t = 10^{-5}$). (a) $k = 5$; (b) $k = 10$; (c) $k = 15$.

Cole has provided the exact solution [6] for this problem in terms of an expansion series which is readily computable roughly for the parameter $\mathrm{Re} \leqslant 100$. In the present DSC treatment, the DSC high-pass filters (12) are used for solving Burgers' equation at $\mathrm{Re} = 100$ as the conjugate low-pass filter is rarely activated at this moderate Reynolds number. The present calculations use 41 grid

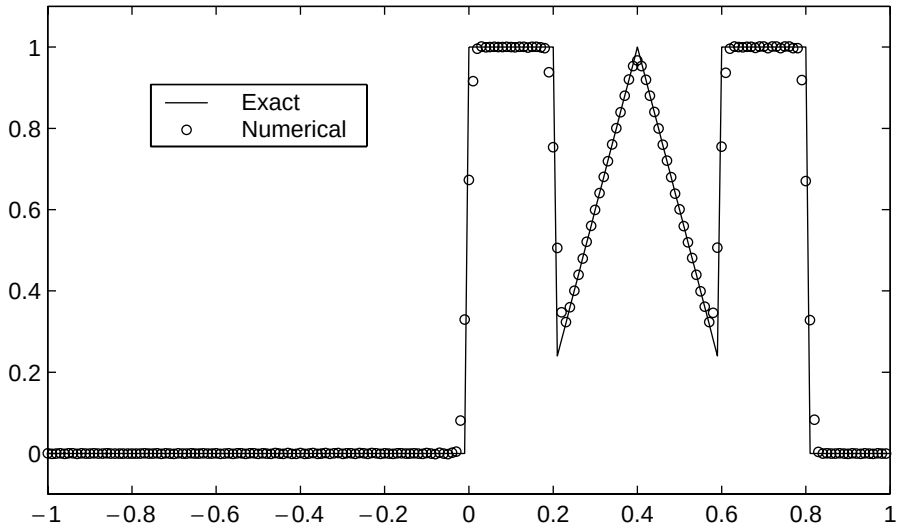

Fig. 3. Linear equation with a discontinuous initial value ($t = 8$, $\Delta x = 0.01$ and $\Delta t/\Delta x = 0.1$).

Table 3
Comparison of errors for solving Burgers' equation

	K–T	DSC	
Time	L_∞	L_∞	L_1
0.4	2.6(− 2)	2.4(− 3)	2.2(− 4)
0.8	2.9(− 2)	3.3(− 3)	2.9(− 4)
1.2	1.8(− 2)	4.7(− 4)	1.1(− 5)
3.0	6.9(− 3)	7.6(− 8)	1.1(− 8)

points in the interval $[0, 1]$. Time increment of 0.01 is used for the time integration. Both L_∞ and L_1 errors at 4 different times are listed in Table 3. In an earlier work, Kakuda and Tosaka [16] tested their generalized boundary element method by using 100 elements, up to 6 iterations and the same time increment as ours ($\Delta t = 0.01$). Their results are also listed in Table 3 for a comparison. The errors in both methods are very small. The DSC results are from 10 to 10^5 times more accurate than those of Kakuda and Tosaka [16](K–T), while the present results are obtained by using much fewer grid points.

The numerical solution of Burgers' equation at a high Reynolds number ($\mathrm{Re} = 10^5$) is very difficult due to the presence of shock [14]. A direct application of the DSC algorithm using 64 grid points ($N = 64$) and a small time increment ($\Delta t = 0.001$) leads to highly oscillatory results as shown in Fig. 4. The time integration is shown up to 0.5 time units and eventually collapses at a later time. The plot is given in the spatial interval of $[0, 2]$, which is generated by an antisymmetric extension of the original numerical results in the spatial interval of $[0, 1]$. The oscillation starts near 0.3 time

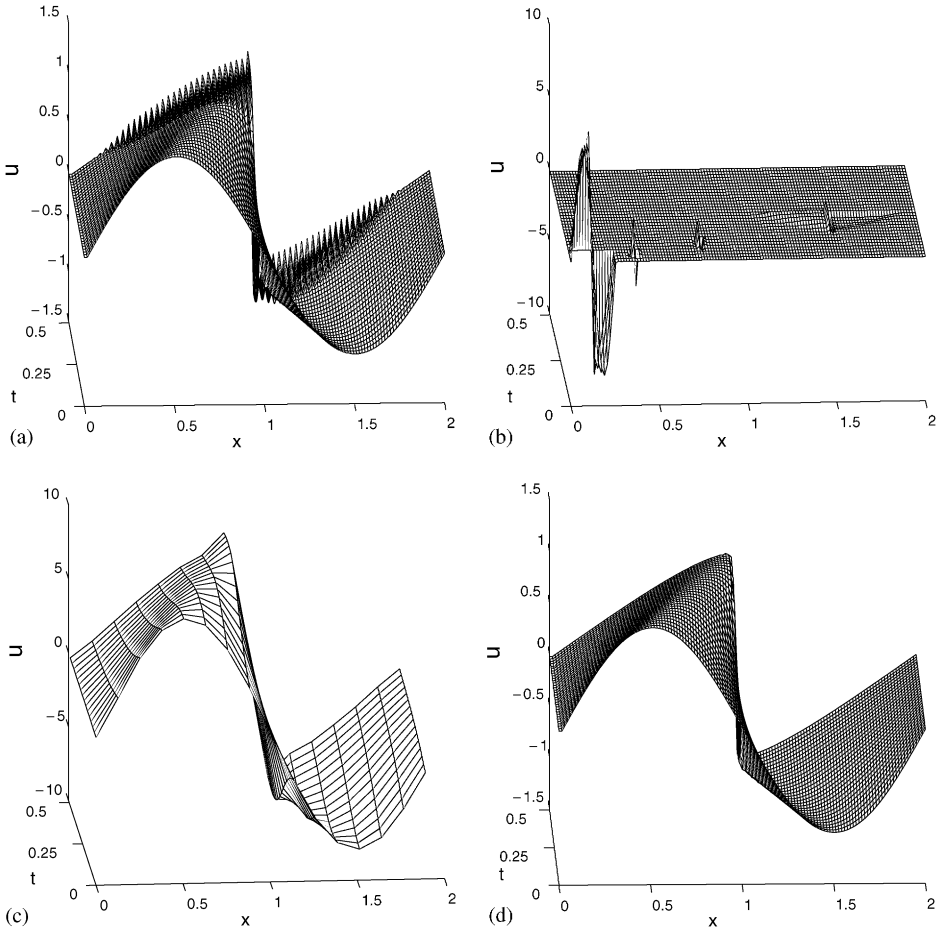

Fig. 4. (a) The oscillatory numerical solution of Burgers' equation ($\mathrm{Re} = 10^5, \Delta t = 0.001, N = 64, t = 0 \sim 0.5$); (b) Three scale wavelet analysis of Fig. 4(a); (c) The last scale low pass response of Fig. 4(b); (d) The CFOR solution of Burgers' equation ($\mathrm{Re} = 10^5, \Delta t = 0.001, N = 64, t = 0 \sim 0.5$).

units and is accumulated and amplified in further integrations. The solid line in Fig. 1 shows the Fourier image of the result at $t = 0.5$. The image has two large peaks, one near the zero and the other near the Nyquist frequency π/Δ.

To analyze Fig. 4(a) further, a three-scale wavelet transform is performed and the result is depicted in Fig. 4(b). Daubechies' biorthogonal wavelets (D7/9) [7] are employed for the wavelet transform. At the first scale, a response extended over a large domain is recorded over the southeast quarter of the quadrangle which corresponds to high frequency oscillations in Fig. 4(a). Note that high frequency oscillations reside exclusively at the southeast quarter of quadrangle because oscillations only occur within a special frequency range. The peak at the middle of the high frequency response region is due to the shock front, which produces two other similar narrow high frequency responses at the second and third scales, respectively. The response of the highest amplitude at the southwest corner is enlarged in Fig. 4(c). Surprisingly, this part seems containing the desired

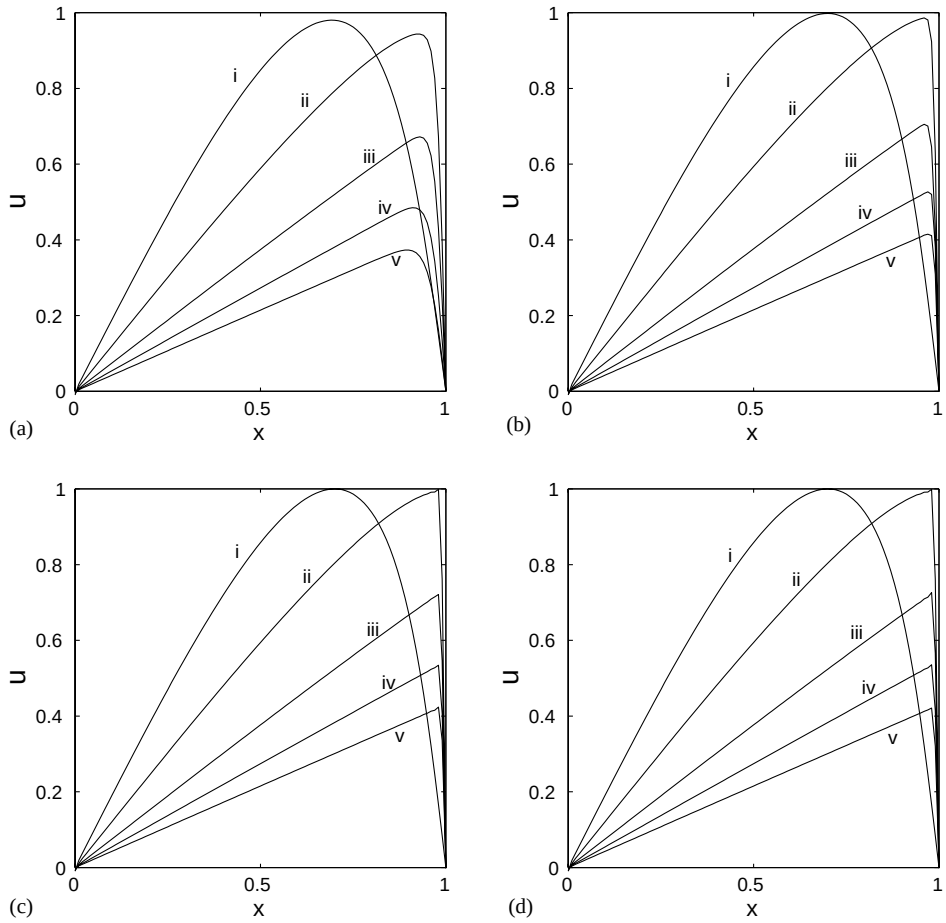

Fig. 5. The CFOR solutions of Burgers' equation at $t=0.2$ (i), 0.5 (ii), 1.0 (iii), 1.5 (iv) and 2.0 (v) ($\Delta t=0.001, N=101$). (a) $\mathrm{Re}=100$; (b) $\mathrm{Re}=10^3$; (c) $\mathrm{Re}=10^5$; (d) $\mathrm{Re}=\infty$.

solution to Burgers' equation. However, there is a kink in the late part of the low pass solution which does not belong to the desired solution. Obviously, had the high frequency oscillations been controlled in the course of integration, such a kink would not have appeared. From this analysis we conclude that the peak near the Nyquist frequency in the Fourier image in Fig. 1 is due to undesired oscillations.

Fig. 4(d) shows the results under the same conditions as those of Fig. 4(a), obtained by using the CFOR scheme. Note that the oscillations are eliminated and meanwhile, a sharp shock profile is resolved. The dotted line in Fig. 1 shows the Fourier image of the solution at time 0.5. It is noted that there is little change to the image inside the effective bandwidth of conjugated filters. However, peaks of high frequency oscillations are effectively eliminated.

We test this scheme for the case of $\mathrm{Re}=10^3$ and 10^5 at $\Delta x=0.01$, $\Delta t=0.001$. As shown in Fig. 5(b) and (c), the CFOR results are excellent. Clearly, all oscillations are effectively removed and the shock front is very sharp. In a dramatic case, we consider inviscid Burgers' equation ($\mathrm{Re}=\infty$).

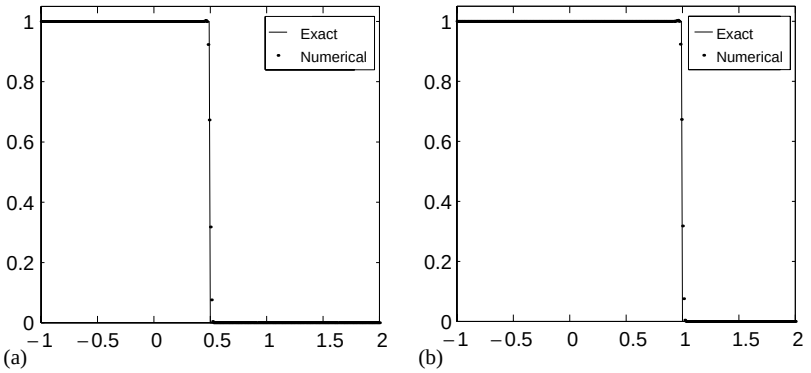

Fig. 6. Inviscid Burgers' equation with shock wave ($\Delta x = 0.01$, $\Delta t/\Delta x = 0.4$). (a) results at $t = 1$, (b) results at $t = 2$.

As depicted in Fig. 5(d), our CFOR scheme works extremely well for this case too. The results for $\mathrm{Re} = 100$ are shown in Fig. 5(a) for a comparison.

Example 2. To test the proposed scheme for solving Burgers' equation further, we next consider the following Riemann type initial value for the inviscid case ($\mathrm{Re} = \infty$)

$$u(x,0) = \begin{cases} 1, & x \leqslant 0, \\ 0, & x > 0. \end{cases} \tag{25}$$

This is a standard benchmark problem in hyperbolic conservation laws and has been considered by many researchers. The exact solution is a shock wave moving with a constant velocity

$$u(x,t) = \begin{cases} 1, & x - St < 0, \\ 0, & x - St > 0, \end{cases} \tag{26}$$

where the speed of the shock front is given by

$$S = \tfrac{1}{2}.$$

The shock wave is compressive in nature. Results of the proposed scheme are depicted in Fig. 6 for two different times. Apparently, the present results are some of the best for solving this problem.

Example 3. Finally, we consider another Riemann type initial value for the inviscid Burgers' equation ($\mathrm{Re} = \infty$)

$$u(x,0) = \begin{cases} 0, & x < 0, \\ 1, & x \geqslant 0. \end{cases} \tag{27}$$

The exact solution of this problem is a rarefaction wave

$$u(x,t) = \begin{cases} 0, & \frac{x}{t} < 0, \\ \frac{x}{t}, & 0 < \frac{x}{t} < 1, \\ 1, & \frac{x}{t} > 1. \end{cases} \tag{28}$$

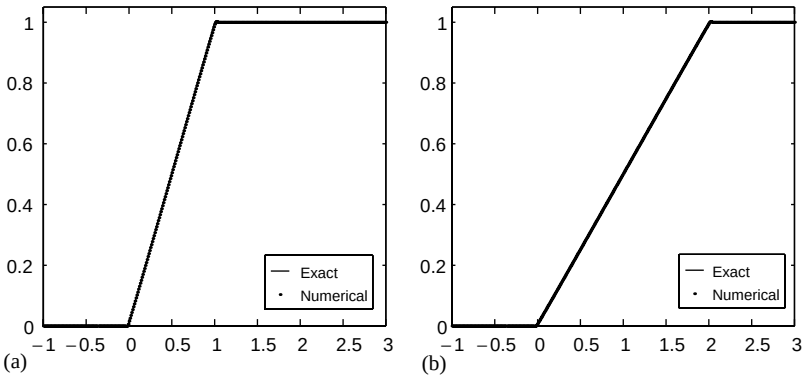

Fig. 7. Inviscid Burgers' equation with rarefaction wave ($\Delta x = 0.01$ and $\Delta t/\Delta x = 0.4$). (a) results at $t = 1$, (b) results at $t = 2$.

The solution is expansive in nature and thus, is a so-called entropy-violating wave. The CFOR results are plotted in Fig. 7 for two different times. Obviously, the present scheme performs extremely well for this case.

4. Conclusion

In conclusion, a novel approach, the conjugate filter oscillation reduction (CFOR) scheme is introduced for solving Burgers' equation with different initial values and Reynolds numbers. The essence of the CFOR scheme is to adaptively implement a conjugate low-pass filter to effectively remove the accumulated numerical errors produced by a set of high-pass filters. The conjugated low-pass and high-pass filters have essentially the same degree of regularity, smoothness, time-frequency localization, effective support and bandwidth. In this work, all conjugated filters are constructed by using discrete singular convolution (DSC) kernels [20].

The numerical accuracy of the CFOR approach is tested by using a linear equation of hyperbolic type with two different initial values. Comparison is made with standard shock-capturing schemes, such as fourth order and fifth order weighted essentially nonoscillatory scheme with Roe's flux splitting and entropy fix (WENO-RF-4 and WENO-RF-5) [15]. The proposed scheme is about 10^{10} times more accuracy than these standard methods. The L_∞ and L_1 numerical orders of the CFOR scheme are about 19 and 22, respectively, in solving this linear wave equation. In fact, much better numerical results are obtained in propagating Gaussian wave packets with the same linear equation. Numerical orders are as high as 30 in resolving the wave packets. We also test the accuracy of the proposed scheme for solving Burgers' equation, for which the analytical solution is readily available at a moderately high Reynolds number ($\mathrm{Re} = 100$). While using much fewer grid points, our results are about 10 to 10^5 times more accurate than those of an accurate finite element approach [16].

The capability of the proposed scheme for shock-capturing is tested on the linear wave equation with contact discontinuities. Such a problem is somewhat difficult to solve in shock capturing. Numerical experiments indicate that the CFOR scheme works extremely well in resolving the shock. Burgers' equation is nonlinear and thus, at high Reynolds number, it produces shock front with a

smooth initial value when the Dirichlet boundary condition is employed. For extremely high Reynolds numbers ($\mathrm{Re} \geqslant 10^5$), the DSC algorithm develops severe oscillations near the shock front. The CFOR scheme can minimize error accumulations and resolve the shock front well. The ability of the CFOR scheme for treating inviscid Burgers' equation is confirmed by taking discontinuous initial values of the Riemann type with periodic boundary conditions. These cases are benchmark problems in hyperbolic conservation laws. Excellent numerical results are obtained for these problems. Therefore, the present CFOR scheme is very accurate and reliable for integrating Burgers' equation over all possible values of Reynolds numbers.

It is noted that the present approach is very general. It can be directly applied to the numerical solution of other partial differential equations, particularly, compressible flows and hyperbolic conservation laws. Moreover, the CFOR scheme can be implemented along with any other standard computational methods, such as high-order central difference schemes, finite element methods and spectral approximations. A detailed discussion of these aspects as well as applications to more general hyperbolic conservation law systems is beyond the scope of the present paper and will be reported elsewhere [10].

Acknowledgements

This work was supported in part by the National University of Singapore.

References

[1] R. Arina, C. Canuto, A self-adaptive domain decomposition for the viscous inviscid coupling 1. Burgers' equation, J. Comput. Phys. 105 (1993) 290–300.
[2] P. Bar-Yoseph, E. Moses, U. Zrahia, A.L. Yarin, Space–time spectral element methods for one-dimensional nonlinear advection–diffusion problems, J. Comput. Phys. 119 (1995) 62–74.
[3] S. Biringen, A. Saati, Comparison of several finite-difference methods, J. Aircraft. 27 (1990) 90–92.
[4] J. Burgers, A Mathematical Model Illustrating the Theory of Turbulence, Advances in Applied Mechanics, Academic Press, New York, 1948.
[5] J. Caldwell, P. Wanless, A.E. Cook, Solutions of Burgers' equation for large Reynolds number using finite elements with moving nodes, J. Appl. Math. Modeling 11 (1987) 211–214.
[6] J.D. Cole, On quasi-linear parabolic equation occurring in aerodynamics, Quart. Appl. Math. 9 (1951) 225–236.
[7] I. Daubechies, Ten Lectures on Wavelets, Society for Industrial and Applied Mathematics, Philadelphia, 1992.
[8] B. Engquist, P. Lötstedt, B. Sjögreen, Nonlinear filters for efficient shock computation, Math. Comput. 186 (1989) 509–537.
[9] S.K. Godunov, Finite difference method for numerical computation of discontinuous solutions to the equations of fluid dynamics, Math. Sb. 47 (1959) 271–306.
[10] Y. Gu, G.W. Wei, Conjugate filter approach for shock capturing, Commun. Numer. Meth. Engng., in press.
[11] A. Harten, B. Engquist, S. Osher, S. Chakravarthy, Uniformly high order accurate essentially non-oscillatory scheme, III, J. Comput. Phys. 71 (1987) 231–303.
[12] Y.C. Hon, X.Z. Mao, An efficient numerical scheme for Burgers' equation, Appl. Math. Comput. 95 (1998) 37–50.
[13] D.H. Jain, D.N. Holla, Numerical solutions of coupled Burgers' equation, Int. J. Non-linear Mech. 13 (1978) 213–222.
[14] P. Jamet, R. Bonnerot, Numerical solution of compressible flow by finite element method which follows the free boundary and the interfaces, J. Comput. Phys. 18 (1975) 21–45.
[15] G.-S. Jiang, C.-W. Shu, Efficient Implementation of Weighted ENO Schemes, J. Comput. Phys. 126 (1996) 202–228.

[16] K. Kakuda, N. Tosaka, The generalized boundary element approach to Burgers' equation, Int. J. Numer. Methods Engng. 29 (1990) 245–261.
[17] H. Nguyen, J. Reynen, in: C. Taylor et al. (Eds.), Numerical Methods for Non-Linear Problems, Proceedings of the International Conference, Vol. 2, Universidal Poltecnica de Barcelona, Spain, Pineridge Press, Swansea, UK, 1984.
[18] E. Varoglu, W.D.L. Finn, Space–time finite elements incorporating characteristics for Burgers' equation, Int. J. Numer. Methods Eng. 16 (1980) 171–184.
[19] D.C. Wan, B.S.V. Patnaik, G.W. Wei, A new benchmark quality solution for the buoyancy driven cavity by discrete singular convolution, Numer. Heat Transfer B—Fundamentals 40 (2001) 199–228.
[20] G.W. Wei, Discrete singular convolution for the solution of the Fokker–Planck equations, J. Chem. Phys. 110 (1999) 8930–8942.
[21] G.W. Wei, A unified approach for solving the Fokker-Planck equation, J. Phys. A 33 (2000) 4935–4953.
[22] G.W. Wei, Wavelet generated by using discrete singular convolution kernels, J. Phys. A 33 (2000) 8577–8596.
[23] G.W. Wei, A new algorithm for solving some mechanical problems, Comput. Methods Appl. Mech. Eng. 190 (2001) 2017–2030.
[24] G.W. Wei, Vibration analysis by discrete singular convolution, J. Sound Vibrat. 244 (2001) 535–553.
[25] G.W. Wei, D.S. Zhang, D.J. Kouri, D.K. Hoffman, Distributed approximating functional approach to Burgers' equation in one and two space dimensions, Comput. Phys. Commun. 111 (1998) 93–109.
[26] Y.B. Zhao, G.W. Wei, Y. Xiang, Discrete singular convolution for the prediction of high frequency vibration of plates, Int. J. Solids Struct. 39 (2002) 65–88.